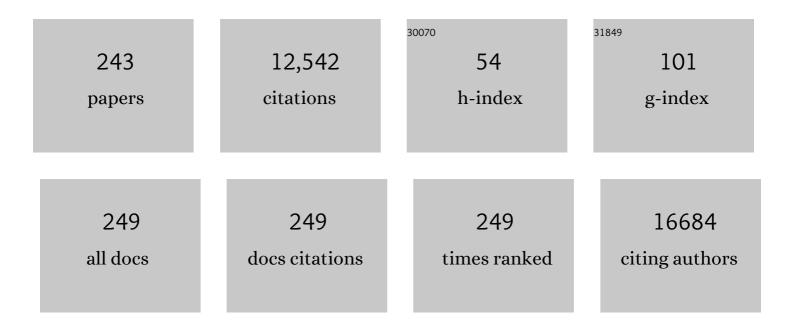
Harry M Meyer

List of Publications by Year in descending order

Source: https://exaly.com/author-pdf/9572088/publications.pdf Version: 2024-02-01



HADDY M MEVED

#	Article	IF	CITATIONS
1	Probing Defect Sites on CeO ₂ Nanocrystals with Well-Defined Surface Planes by Raman Spectroscopy and O ₂ Adsorption. Langmuir, 2010, 26, 16595-16606.	3.5	889
2	Characterizing the Li–Li7La3Zr2O12 interface stability and kinetics as a function of temperature and current density. Journal of Power Sources, 2016, 302, 135-139.	7.8	446
3	Band Gap Narrowing of Titanium Oxide Semiconductors by Noncompensated Anion-Cation Codoping for Enhanced Visible-Light Photoactivity. Physical Review Letters, 2009, 103, 226401.	7.8	347
4	Studies on Supercapacitor Electrode Material from Activated Lignin-Derived Mesoporous Carbon. Langmuir, 2014, 30, 900-910.	3.5	342
5	Creep-Resistant, Al2O3-Forming Austenitic Stainless Steels. Science, 2007, 316, 433-436.	12.6	337
6	lmpact of air exposure and surface chemistry on Li–Li ₇ La ₃ Zr ₂ O ₁₂ interfacial resistance. Journal of Materials Chemistry A, 2017, 5, 13475-13487.	10.3	300
7	A physical catalyst for the electrolysis of nitrogen to ammonia. Science Advances, 2018, 4, e1700336.	10.3	264
8	Highâ€Selectivity Electrochemical Conversion of CO ₂ to Ethanol using a Copper Nanoparticle/Nâ€Doped Graphene Electrode. ChemistrySelect, 2016, 1, 6055-6061.	1.5	251
9	Large scale atmospheric pressure chemical vapor deposition of graphene. Carbon, 2013, 54, 58-67.	10.3	241
10	Nanofibrous chitosan non-wovens for filtration applications. Polymer, 2009, 50, 3661-3669.	3.8	234
11	Synthesis of Hexagonal Boron Nitride Monolayer: Control of Nucleation and Crystal Morphology. Chemistry of Materials, 2015, 27, 8041-8047.	6.7	202
12	Rapid tarnishing of silver nanoparticles in ambient laboratory air. Applied Physics B: Lasers and Optics, 2005, 80, 915-921.	2.2	190
13	Thin intergranular films and solid-state activated sintering in nickel-doped tungsten. Acta Materialia, 2007, 55, 3131-3142.	7.9	190
14	Nature of the band gap and origin of the electro-/photo-activity of Co3O4. Journal of Materials Chemistry C, 2013, 1, 4628.	5.5	176
15	lonic Liquids as Novel Lubricants and Additives for Diesel Engine Applications. Tribology Letters, 2009, 35, 181-189.	2.6	168
16	Synergistic Effects Between Phosphoniumâ€Alkylphosphate Ionic Liquids and Zinc Dialkyldithiophosphate (ZDDP) as Lubricant Additives. Advanced Materials, 2015, 27, 4767-4774.	21.0	168
17	Phosphonium-Organophosphate Ionic Liquids as Lubricant Additives: Effects of Cation Structure on Physicochemical and Tribological Characteristics. ACS Applied Materials & Interfaces, 2014, 6, 22585-22593.	8.0	163
18	Uniform corrosion of FeCrAl alloys in LWR coolant environments. Journal of Nuclear Materials, 2016, 479, 36-47.	2.7	158

#	Article	IF	CITATIONS
19	Chemical stability and long-term cell performance of low-cobalt, Ni-Rich cathodes prepared by aqueous processing for high-energy Li-Ion batteries. Energy Storage Materials, 2020, 24, 188-197.	18.0	155
20	Thermally nitrided stainless steels for polymer electrolyte membrane fuel cell bipolar plates. Journal of Power Sources, 2004, 138, 79-85.	7.8	142
21	Monodispersed biocompatible silver sulfide nanoparticles: Facile extracellular biosynthesis using the γ-proteobacterium, Shewanella oneidensis. Acta Biomaterialia, 2011, 7, 4253-4258.	8.3	138
22	Low Energy Implantation into Transition-Metal Dichalcogenide Monolayers to Form Janus Structures. ACS Nano, 2020, 14, 3896-3906.	14.6	136
23	Segregation-induced grain boundary premelting in nickel-doped tungsten. Applied Physics Letters, 2005, 87, 231902.	3.3	133
24	Electrical and thermal conductivity of low temperature CVD graphene: the effect of disorder. Nanotechnology, 2011, 22, 275716.	2.6	132
25	Methanol Fractionation of Softwood Kraft Lignin: Impact on the Lignin Properties. ChemSusChem, 2014, 7, 221-228.	6.8	132
26	Tribological characteristics of aluminum alloys sliding against steel lubricated by ammonium and imidazolium ionic liquids. Wear, 2009, 267, 1226-1231.	3.1	125
27	Nitrogen-enriched ordered mesoporous carbons through direct pyrolysis in ammonia with enhanced capacitive performance. Journal of Materials Chemistry A, 2013, 1, 7920.	10.3	120
28	Aluminum/polyimide interface formation: An xâ€ray photoelectron spectroscopy study of selective chemical bonding. Journal of Vacuum Science and Technology A: Vacuum, Surfaces and Films, 1987, 5, 3325-3333.	2.1	117
29	Transmission Electron Microscopy Study of Aqueous Film Formation and Evolution on Magnesium Alloys. Journal of the Electrochemical Society, 2014, 161, C302-C311.	2.9	111
30	Effect of tungsten crystallographic orientation on He-ion-induced surface morphology changes. Acta Materialia, 2014, 62, 173-181.	7.9	109
31	Tertiary and Quaternary Ammonium-Phosphate Ionic Liquids as Lubricant Additives. Tribology Letters, 2016, 63, 1.	2.6	107
32	Electronic structures of theYBa2Cu3O7â^'xsurface and its modification by sputtering and adatoms of Ti and Cu. Physical Review B, 1988, 38, 6500-6512.	3.2	104
33	Responses of bone-forming cells on pre-immersed Zr-based bulk metallic glasses: Effects of composition and roughness. Acta Biomaterialia, 2011, 7, 395-405.	8.3	102
34	Valence bands, oxygen in planes and chains, and surface changes for single crystals ofM2CuO4andMBa2Cu3Ox(M=Pr,Nd,Eu,Gd). Physical Review B, 1988, 38, 4668-4676.	3.2	101
35	Characteristics of wear particles produced during friction tests of conventional and unconventional disc brake materials. Wear, 2003, 255, 1261-1269.	3.1	94
36	Corrosion behavior of CrN, Cr2N and π phase surfaces on nitrided Ni–50Cr for proton exchange membrane fuel cell bipolar plates. Corrosion Science, 2006, 48, 3157-3171.	6.6	92

#	Article	IF	CITATIONS
37	Organic-Modified Silver Nanoparticles as Lubricant Additives. ACS Applied Materials & Interfaces, 2017, 9, 37227-37237.	8.0	90
38	Photoinduced Strong Metal–Support Interaction for Enhanced Catalysis. Journal of the American Chemical Society, 2021, 143, 8521-8526.	13.7	85
39	Hydrothermal corrosion of SiC in LWR coolant environments in theÂabsence of irradiation. Journal of Nuclear Materials, 2015, 465, 488-498.	2.7	84
40	Occupied electronic states of single-crystalBi2Ca1+xSr2â^'xCu2O8+y. Physical Review B, 1988, 38, 7144-7147.	3.2	83
41	Defect-Mediated Phase Transformation in Anisotropic Two-Dimensional PdSe ₂ Crystals for Seamless Electrical Contacts. Journal of the American Chemical Society, 2019, 141, 8928-8936.	13.7	81
42	Surpassing Robeson Upper Limit for CO2/N2 Separation with Fluorinated Carbon Molecular Sieve Membranes. CheM, 2020, 6, 631-645.	11.7	73
43	Degradation of SS316L bipolar plates in simulated fuel cell environment: Corrosion rate, barrier film formation kinetics and contact resistance. Journal of Power Sources, 2015, 273, 1237-1249.	7.8	69
44	Powder bed charging during electron-beam additive manufacturing. Acta Materialia, 2017, 124, 437-445.	7.9	69
45	Properties of thermo-chemically surface treated carbon fibers and of their epoxy and vinyl ester composites. Composites Part A: Applied Science and Manufacturing, 2012, 43, 1120-1133.	7.6	68
46	Unraveling the Molecular Weight Dependence of Interfacial Interactions in Poly(2-vinylpyridine)/Silica Nanocomposites. ACS Macro Letters, 2017, 6, 68-72.	4.8	65
47	Electrolyte Volume Effects on Electrochemical Performance and Solid Electrolyte Interphase in Si-Graphite/NMC Lithium-Ion Pouch Cells. ACS Applied Materials & Interfaces, 2017, 9, 18799-18808.	8.0	65
48	Selecting the Best Graphite for Long-Life, High-Energy Li-Ion Batteries. Journal of the Electrochemical Society, 2018, 165, A1837-A1845.	2.9	65
49	Oxygenâ€Functionalized Fewâ€Layer Graphene Sheets as Active Catalysts for Oxidative Dehydrogenation Reactions. ChemSusChem, 2013, 6, 840-846.	6.8	61
50	Lithium and transition metal dissolution due to aqueous processing in lithium-ion battery cathode active materials. Journal of Power Sources, 2020, 466, 228315.	7.8	61
51	High performance Cr, N-codoped mesoporous TiO ₂ microspheres for lithium-ion batteries. Journal of Materials Chemistry A, 2014, 2, 1818-1824.	10.3	58
52	High-Resolution Soft X-ray Photoelectron Spectroscopic Studies and Scanning Auger Microscopy Studies of the Air Oxidation of Alkylated Silicon(111) Surfaces. Journal of Physical Chemistry B, 2006, 110, 23450-23459.	2.6	57
53	Passivation of highTcsuperconductor surfaces with CaF2and Bi, Al, and Si oxides. Applied Physics Letters, 1988, 53, 1657-1659.	3.3	56
54	Oxidative dehydrogenation of isobutane on phosphorous-modified graphitic mesoporous carbon. Carbon, 2011, 49, 659-668.	10.3	56

#	Article	IF	CITATIONS
55	Balancing formation time and electrochemical performance of high energy lithium-ion batteries. Journal of Power Sources, 2018, 402, 107-115.	7.8	56
56	Fabrication and characterization of brookite-rich, visible light-active TiO2 films for water splitting. Applied Catalysis B: Environmental, 2009, 93, 90-95.	20.2	54
57	Corrosion of CVD Silicon Carbide in 500°C Supercritical Water. Journal of the American Ceramic Society, 2007, 90, 315-318.	3.8	53
58	Properties of ultrafast laser textured silicon for photovoltaics. Solar Energy Materials and Solar Cells, 2011, 95, 2745-2751.	6.2	53
59	Nanostructure and Composition of Tribo-Boundary Films Formed in Ionic Liquid Lubrication. Tribology Letters, 2011, 43, 205-211.	2.6	53
60	Experimental secondary electron spectra under SEM conditions. Journal of Microscopy, 2004, 215, 77-85.	1.8	52
61	Photoemission and inverse resonant photoemission studies ofTl2Ba2Ca2Cu3O10+y. Physical Review B, 1989, 39, 7343-7346.	3.2	51
62	Singleâ€crystal YBa2Cu3O7â^'xand Bi2Ca1+xSr2â^'xCu2O8+ysurfaces and Ag adatomâ€induced modification. Journal of Applied Physics, 1989, 65, 3130-3135.	2.5	51
63	Evaluation of nitrided titanium separator plates for proton exchange membrane electrolyzer cells. Journal of Power Sources, 2014, 272, 954-960.	7.8	51
64	Improving microstructure of silicon/carbon nanofiber composites as a Li battery anode. Journal of Power Sources, 2013, 221, 455-461.	7.8	50
65	Advanced surface and microstructural characterization of natural graphite anodes for lithium ion batteries. Carbon, 2014, 72, 393-401.	10.3	50
66	Evaluation of Gas Formation and Consumption Driven by Crossover Effect in High-Voltage Lithium-Ion Batteries with Ni-Rich NMC Cathodes. ACS Applied Materials & Interfaces, 2019, 11, 43235-43243.	8.0	50
67	Controlling thin film structure for the dewetting of catalyst nanoparticle arrays for subsequent carbon nanofiber growth. Nanotechnology, 2007, 18, 465304.	2.6	49
68	Scalable production of microbially mediated zinc sulfide nanoparticles and application to functional thin films. Acta Biomaterialia, 2014, 10, 4474-4483.	8.3	49
69	Characterization of ZDDP and ionic liquid tribofilms on non-metallic coatings providing insights of tribofilm formation mechanisms. Wear, 2015, 332-333, 1273-1285.	3.1	48
70	A study of the corrosion behaviour of Zr50Cu(40â^'X)Al10PdX bulk metallic glasses with scanning Auger microanalysis. Corrosion Science, 2008, 50, 1825-1832.	6.6	47
71	Bis(trimethylsilyl) 2-fluoromalonate derivatives as electrolyte additives for high voltage lithium ion batteries. Journal of Power Sources, 2019, 412, 527-535.	7.8	47
72	Fabrication and Characterization of Carbon Nanofiber-Based Vertically Integrated Schottky Barrier Junction Diodes. Nano Letters, 2003, 3, 1751-1755.	9.1	46

#	Article	IF	CITATIONS
73	Scalable superhydrophobic coatings based on fluorinated diatomaceous earth: Abrasion resistance versus particle geometry. Applied Surface Science, 2014, 292, 563-569.	6.1	46
74	Direct Characterization of Atomically Dispersed Catalysts: Nitrogenâ€Coordinated Ni Sites in Carbonâ€Based Materials for CO ₂ Electroreduction. Advanced Energy Materials, 2020, 10, 2001836.	19.5	46
75	Y, Ba, Cu, and Ti interface reactions with SrTiO3(100) surfaces. Journal of Applied Physics, 1989, 65, 4943-4950.	2.5	44
76	Influence of the carbon fiber surface microstructure on the surface chemistry generated by a thermo-chemical surface treatment. Applied Surface Science, 2012, 261, 473-480.	6.1	44
77	Comparison of the tribological behavior of steel–steel and Si3N4–steel contacts in lubricants with ZDDP or ionic liquid. Wear, 2014, 319, 172-183.	3.1	43
78	Structural Interconversion between Agglomerated Palladium Domains and Mononuclear Pd(II) Cations in Chabazite Zeolites. Chemistry of Materials, 2021, 33, 1698-1713.	6.7	42
79	Photoemission and inverse-photoemission studies ofBa1â^'xKxBiO3â^'y. Physical Review B, 1989, 40, 4532-4537.	3.2	41
80	Ba oxides: Core level binding energies and defect-related Fermi level pinning. Surface Science, 1990, 225, 63-71.	1.9	41
81	Microanalysis of alkali-activated fly ash–CH pastes. Cement and Concrete Research, 2002, 32, 963-972.	11.0	41
82	Cu–Ni composition gradient for the catalytic synthesis of vertically aligned carbon nanofibers. Carbon, 2005, 43, 1857-1863.	10.3	41
83	Single-crystal nanowires grown via electron-beam-induced deposition. Nanotechnology, 2008, 19, 345705.	2.6	41
84	Oxygen diffusion enables anti-wear boundary film formation on titanium surfaces in zinc-dialkyl-dithiophosphate (ZDDP)-containing lubricants. Scripta Materialia, 2009, 60, 886-889.	5.2	41
85	Pre-oxidized and nitrided stainless steel alloy foil for proton exchange membrane fuel cell bipolar plates: Part 1. Corrosion, interfacial contact resistance, and surface structure. Journal of Power Sources, 2010, 195, 5610-5618.	7.8	41
86	Improving corrosion resistance of AZ31B magnesium alloy via a conversion coating produced by a protic ammonium-phosphate ionic liquid. Thin Solid Films, 2014, 568, 44-51.	1.8	41
87	Influence of Surface Oxidation on Ion Dynamics and Capacitance in Porous and Nonporous Carbon Electrodes. Journal of Physical Chemistry C, 2016, 120, 8730-8741.	3.1	40
88	Toward the Design of a Hierarchical Perovskite Support: Ultra-Sintering-Resistant Gold Nanocatalysts for CO Oxidation. ACS Catalysis, 2017, 7, 3388-3393.	11.2	40
89	Influence of Atomic Layer Deposition Temperatures on TiO ₂ /n-Si MOS Capacitor. ECS Journal of Solid State Science and Technology, 2013, 2, N110-N114.	1.8	39
90	Size tunable elemental copper nanoparticles: extracellular synthesis by thermoanaerobic bacteria and capping molecules. Journal of Materials Chemistry C, 2015, 3, 644-650.	5.5	39

#	Article	IF	CITATIONS
91	Identifying degradation mechanisms in lithium-ion batteries with coating defects at the cathode. Applied Energy, 2018, 231, 446-455.	10.1	39
92	Depolymerization of corn stover lignin with bulk molybdenum carbide catalysts. Fuel, 2019, 244, 528-535.	6.4	39
93	Xâ€ray photoemission investigations of clustering and electron emission, injection, and trapping at the gold/polyimide interface. Journal of Vacuum Science and Technology A: Vacuum, Surfaces and Films, 1988, 6, 30-37.	2.1	38
94	Cu adatom interactions with single- and polycrystallineBi2Ca1+xSr2â^'xCu2O8+yandYBa2Cu3O7â^'x. Physical Review B, 1988, 38, 11331-11336.	3.2	38
95	Effects of pretreatment and process temperature of a conversion coating produced by an aprotic ammonium-phosphate ionic liquid on magnesium corrosion protection. Electrochimica Acta, 2014, 123, 58-65.	5.2	38
96	Reactivity and passivation for Bi adatoms on YBa2Cu3O6.9and Bi2Ca1+xSr2â^'xCu2O8+y. Applied Physics Letters, 1988, 53, 1004-1006.	3.3	37
97	Effect of chain length on nanomechanics of alkanethiol self-assembly. Nanotechnology, 2007, 18, 424028.	2.6	37
98	Comparing Cr, and N only doping with (Cr, N)-codoping for enhancing visible light reactivity of TiO2. Applied Catalysis B: Environmental, 2011, 110, 148-153.	20.2	37
99	Dynamics of polyimide curing and degradation: An in situ xâ€ray photoemission study. Journal of Vacuum Science and Technology A: Vacuum, Surfaces and Films, 1988, 6, 38-43.	2.1	36
100	Influence of thermal history on the mechanical properties of carbon fiber–acrylate composites cured by electron beam and thermal processes. Composites Part A: Applied Science and Manufacturing, 2013, 45, 162-172.	7.6	36
101	Ultralow Boundary Lubrication Friction by Three-Way Synergistic Interactions among Ionic Liquid, Friction Modifier, and Dispersant. ACS Applied Materials & Interfaces, 2020, 12, 17077-17090.	8.0	36
102	Oxygen withdrawal, copper valency, and interface reaction for Fe/La1.85Sr0.15CuO4. Physical Review B, 1987, 36, 3979-3982.	3.2	35
103	A dicyanobenzoquinone based cathode material for rechargeable lithium and sodium ion batteries. Journal of Materials Chemistry A, 2019, 7, 17888-17895.	10.3	35
104	Temperatureâ€dependent xâ€ray photoemission studies of metastable Co/polyimide interface formation. Journal of Vacuum Science and Technology A: Vacuum, Surfaces and Films, 1988, 6, 2205-2212.	2.1	34
105	Manufacturing and performance assessment of stamped, laser welded, and nitrided FeCrV stainless steel bipolar plates for proton exchange membrane fuel cells. International Journal of Hydrogen Energy, 2013, 38, 4734-4739.	7.1	34
106	Interfacial Reactions and Performance of Li ₇ La ₃ Zr ₂ O ₁₂ -Stabilized Li–Sulfur Hybrid Cell. ACS Applied Materials & Interfaces, 2019, 11, 42042-42048.	8.0	34
107	Enabling aqueous processing for LiNi0.80Co0.15Al0.05O2 (NCA)-based lithium-ion battery cathodes using polyacrylic acid. Electrochimica Acta, 2021, 380, 138203.	5.2	33
108	MoS2 nanosheet integrated electrodes with engineered 1T-2H phases and defects for efficient hydrogen production in practical PEM electrolysis. Applied Catalysis B: Environmental, 2022, 313, 121458.	20.2	33

#	Article	IF	CITATIONS
109	Immobilization of Biomolecules on Poly(vinyldimethylazlactone)-Containing Surface Scaffolds. Langmuir, 2009, 25, 262-268.	3.5	32
110	Compatibility between Various Ionic Liquids and an Organic Friction Modifier as Lubricant Additives. Langmuir, 2018, 34, 10711-10720.	3.5	31
111	Spectroscopic evidence for passivation of the La1.85Sr0.15CuO4surface with gold. Applied Physics Letters, 1987, 51, 1118-1120.	3.3	30
112	Scuffing transition diagrams for heavy duty diesel fuel injector materials in ultra low-sulfur fuel-lubricated environment. Wear, 2005, 259, 1031-1040.	3.1	30
113	Role of Surface Functionality in the Electrochemical Performance of Silicon Nanowire Anodes for Rechargeable Lithium Batteries. ACS Applied Materials & Interfaces, 2014, 6, 7607-7614.	8.0	30
114	Anti-soiling and highly transparent coatings with multi-scale features. Solar Energy Materials and Solar Cells, 2018, 188, 255-262.	6.2	30
115	Al2O3/TiO2 coated separators: Roll-to-roll processing and implications for improved battery safety and performance. Journal of Power Sources, 2021, 507, 230259.	7.8	30
116	Microstructural stability of copper with antimony dopants at grain boundaries: experiments and molecular dynamics simulations. Journal of Materials Science, 2010, 45, 6707-6718.	3.7	29
117	Effect of GaN surface treatment on Al2O3/ <i>n</i> -GaN MOS capacitors. Journal of Vacuum Science and Technology B:Nanotechnology and Microelectronics, 2015, 33, .	1.2	29
118	Fluorination of MXene by Elemental F ₂ as Electrode Material for Lithiumâ€lon Batteries. ChemSusChem, 2019, 12, 1316-1324.	6.8	28
119	The corrosion and passivity of sputtered Mg–Ti alloys. Corrosion Science, 2016, 104, 36-46.	6.6	27
120	O 2pholes: Temperature effects and surface characteristics of cuprate superconductors. Physical Review B, 1990, 41, 4201-4211.	3.2	26
121	Crystal growth of B12As2 on SiC substrate by CVD method. Journal of Crystal Growth, 2005, 273, 431-438.	1.5	26
122	Molybdenum Carbides, Active and <i>In Situ</i> Regenerable Catalysts in Hydroprocessing of Fast Pyrolysis Bio-Oil. Energy & Fuels, 2016, 30, 5016-5026.	5.1	26
123	Palladium Nanoparticle-Enabled Ultrathick Tribofilm with Unique Composition. ACS Applied Materials & Interfaces, 2018, 10, 31804-31812.	8.0	26
124	Low-Cost Transformation of Biomass-Derived Carbon to High-Performing Nano-graphite via Low-Temperature Electrochemical Graphitization. ACS Applied Materials & Interfaces, 2021, 13, 4393-4401.	8.0	26
125	Cu-induced surface disruption ofLa1.85Sr0.15CuO4. Physical Review B, 1988, 37, 511-514.	3.2	25
126	Thermal stability of HfO2 nanotube arrays. Applied Surface Science, 2011, 257, 4075-4081.	6.1	25

#	Article	IF	CITATIONS
127	Advanced characterization study of commercial conversion and electrocoating structures on magnesium alloys AZ31B and ZE10A. Surface and Coatings Technology, 2016, 294, 164-176.	4.8	25
128	Growth and Electrochemical Characterization of Carbon Nanospike Thin Film Electrodes. Journal of the Electrochemical Society, 2014, 161, H558-H563.	2.9	24
129	X-ray photoelectron spectroscopy of uv laser irradiated sapphire and alumina. Journal of Materials Research, 1994, 9, 2251-2257.	2.6	23
130	Characterization of zirconium carbides using electron microscopy, optical anisotropy, Auger depth profiles, X-ray diffraction, and electron density calculated by charge flipping method. Journal of Solid State Chemistry, 2012, 194, 91-99.	2.9	23
131	Reâ€establishing the paradigm for evaluating halide salt compatibility to study commercial chloride salts at 600°C–800°C. Materials and Corrosion - Werkstoffe Und Korrosion, 2019, 70, 1439-1449.	1.5	23
132	Ionic liquids as oil additives for lubricating oxygen-diffusion case-hardened titanium. Tribology International, 2019, 136, 342-348.	5.9	23
133	Wet oxidation of stainless steels: New insights into hydrogen ingress. Corrosion Science, 2011, 53, 1633-1638.	6.6	22
134	Lattice Matched Carbide–Phosphide Composites with Superior Electrocatalytic Activity and Stability. Chemistry of Materials, 2017, 29, 9369-9377.	6.7	22
135	New synthesis strategies to improve Co-Free LiNi0.5Mn0.5O2 cathodes: Early transition metal d0 dopants and manganese pyrophosphate coating. Journal of Power Sources, 2020, 479, 228591.	7.8	22
136	Sputtering of lunar regolith simulant by protons and singly and multicharged Ar ions at solar wind energies. Nuclear Instruments & Methods in Physics Research B, 2011, 269, 1316-1320.	1.4	21
137	Development of Cast Alumina-Forming Austenitic Stainless Steels. Jom, 2016, 68, 2803-2810.	1.9	21
138	Solvent-Mediated Synthesis of Amorphous Li ₃ PS ₄ /Polyethylene Oxide Composite Solid Electrolytes with High Li ⁺ Conductivity. Chemistry of Materials, 2020, 32, 8789-8797.	6.7	21
139	Modified coal char materials with high rate performance for battery applications. Carbon, 2021, 172, 414-421.	10.3	21
140	Polymer, Additives, and Processing Effects on N95 Filter Performance. ACS Applied Polymer Materials, 2021, 3, 1022-1031.	4.4	21
141	Na _{1+<i>x</i>} Mn _{<i>x</i>/2} Zr _{2–<i>x</i>/2} (PO ₄) _{3as a Li⁺ and Na⁺ Super Ion Conductor for Solid-State Batteries. ACS Energy Letters, 2021, 6, 429-436.}	ub> 17.4	20
142	Titaniumâ€oxygen reaction at the Ti/La1.85Sr0.15CuO4interface. Applied Physics Letters, 1987, 51, 1750-1752.	3.3	19
143	Compatibility of FeCrAlMo with flowing PbLi at 500°-650â€ ⁻ °C. Journal of Nuclear Materials, 2020, 528, 151847.	2.7	19
144	Electronic Structure and Band Alignment at an Epitaxial Spinel/Perovskite Heterojunction. ACS Applied Materials & Interfaces, 2014, 6, 14338-14344.	8.0	18

#	Article	IF	CITATIONS
145	Compositional tuning of the strain-induced structural phase transition and of ferromagnetism in Bi _{1â°'<i>x</i>} Ba <i>_x</i> FeO _{3â^'<i>δ</i>} . Journal of Materials Research, 2011, 26, 1326-1331.	2.6	17
146	Direct Electrodeposition of UO2 from Uranyl Bis(trifluoromethanesulfonyl)imide Dissolved in 1-Ethyl-3-methylimidazolium Bis(trifluoromethanesulfonyl)imide Room Temperature Ionic Liquid System. Electrochimica Acta, 2014, 115, 630-638.	5.2	17
147	Sulfur-Tolerant Molybdenum Carbide Catalysts Enabling Low-Temperature Stabilization of Fast Pyrolysis Bio-oil. Energy & Fuels, 2017, 31, 9585-9594.	5.1	17
148	Nitrogen impurity gettering in oxide dispersion ductilized chromium. Materials Science & Engineering A: Structural Materials: Properties, Microstructure and Processing, 2003, 358, 243-254.	5.6	16
149	Empty electronic states of graphite and the growth of Au and Pd clusters. Physical Review B, 1988, 38, 3037-3044.	3.2	15
150	Semiconductor/polyimide interface formation: An xâ€ray photoelectron spectroscopy study of germanium chemical bonding. Journal of Vacuum Science and Technology A: Vacuum, Surfaces and Films, 1988, 6, 2175-2181.	2.1	15
151	Photoemission, inverse photoemission, and ab initio SCF investigations of the electronic structure of polyimide. Chemical Physics Letters, 1989, 164, 527-532.	2.6	15
152	Surface microstructuring and long-range ordering of silicon nanoparticles. Applied Physics Letters, 2002, 80, 3799-3801.	3.3	15
153	The Durability of Various Crucible Materials for Aluminum Nitride Crystal Growth by Sublimation. MRS Internet Journal of Nitride Semiconductor Research, 2004, 9, 1.	1.0	15
154	Surface modification and chemical sputtering of graphite induced by low-energy atomic and molecular deuterium ions. Vacuum, 2008, 82, 1285-1290.	3.5	15
155	Aging of nanocarbons in ambient conditions: Probable metastability of carbon nanotubes. Journal of Colloid and Interface Science, 2009, 338, 128-134.	9.4	15
156	Nanostructured columnar heterostructures of TiO2 and Cu2O enabled by a thin-film self-assembly approach: Potential for photovoltaics. Materials Research Bulletin, 2013, 48, 352-356.	5.2	15
157	He-ion and self-atom induced damage and surface-morphology changes of a hot W target. Physica Scripta, 2014, T159, 014029.	2.5	15
158	Does the Use of Diamond‣ike Carbon Coating and Organophosphate Lubricant Additive Together Cause Excessive Tribochemical Material Removal?. Advanced Materials Interfaces, 2015, 2, 1500213.	3.7	15
159	Ion-gated carbon molecular sieve gas separation membranes. Journal of Membrane Science, 2020, 604, 118013.	8.2	15
160	Chromium evaporation and oxidation characteristics of alumina-forming austenitic stainless steels for balance of plant applications in solid oxide fuel cells. International Journal of Hydrogen Energy, 2021, 46, 21619-21633.	7.1	15
161	Operando Analysis of Gas Evolution in TiNb ₂ O ₇ (TNO)-Based Anodes for Advanced High-Energy Lithium-Ion Batteries under Fast Charging. ACS Applied Materials & Interfaces, 2021, 13, 55145-55155.	8.0	15
162	Anorthite sputtering by H ⁺ and Ar ^{<i>q</i>+} (<i>q</i> = 1–9) at solar wind velocities. Journal of Geophysical Research: Space Physics, 2014, 119, 8006-8016.	2.4	14

#	Article	IF	CITATIONS
163	Structural Evolution of Molybdenum Carbides in Hot Aqueous Environments and Impact on Low-Temperature Hydroprocessing of Acetic Acid. Catalysts, 2015, 5, 406-423.	3.5	14
164	Effect of friction stir welding and post-weld heat treatment on a nanostructured ferritic alloy. Journal of Nuclear Materials, 2016, 469, 200-208.	2.7	14
165	Rapid Diffusion and Nanosegregation of Hydrogen in Magnesium Alloys from Exposure to Water. ACS Applied Materials & Interfaces, 2017, 9, 38125-38134.	8.0	14
166	Styrene-Based Elastomer Composites with Functionalized Graphene Oxide and Silica Nanofiber Fillers: Mechanical and Thermal Conductivity Properties. Nanomaterials, 2020, 10, 1682.	4.1	14
167	Effective Strategy for Improving Electrocatalyst Durability by Adhesive Immobilization of Catalyst Nanoparticles on Graphitic Carbon Supports. ACS Catalysis, 2015, 5, 3662-3674.	11.2	13
168	<i>In situ</i> capping for size control of monochalcogenide (ZnS, CdS and SnS) nanocrystals produced by anaerobic metal-reducing bacteria. Nanotechnology, 2015, 26, 325602.	2.6	13
169	Highâ€Voltage Performance of Niâ€Rich NCA Cathodes: Linking Operating Voltage with Cathode Degradation. ChemElectroChem, 2019, 6, 5571-5580.	3.4	13
170	Formation of LiF Surface Layer During Direct Fluorination of High-Capacity Co-Free Disordered Rocksalt Cathodes. ACS Applied Materials & Interfaces, 2021, 13, 38221-38228.	8.0	13
171	Summary Abstract: Xâ€ray photoemission investigation of electron injection and trapping at the gold/polyimide interface. Journal of Vacuum Science and Technology A: Vacuum, Surfaces and Films, 1988, 6, 1002-1004.	2.1	12
172	Insulating gallium oxide layer produced by thermal oxidation of galliumâ€polar GaN. Physica Status Solidi C: Current Topics in Solid State Physics, 2014, 11, 565-568.	0.8	12
173	Synergistic Interactions Between Silver and Palladium Nanoparticles in Lubrication. ACS Applied Nano Materials, 2019, 2, 5302-5309.	5.0	12
174	Magnesium Alloy Effects on Plasma Electrolytic Oxidation Electro-Ceramic and Electro-Coat Formation and Corrosion Resistance. Journal of the Electrochemical Society, 2019, 166, C492-C508.	2.9	12
175	Synthesizing Highâ€Capacity Oxyfluoride Conversion Anodes by Direct Fluorination of Molybdenum Dioxide (MoO ₂). ChemSusChem, 2020, 13, 3825-3834.	6.8	12
176	Interaction of beryllium with 316H stainless steel in molten Li2BeF4 (FLiBe). Journal of Nuclear Materials, 2022, 565, 153698.	2.7	12
177	Silicon interfaces with high temperature superconductors. Surface Science, 1990, 236, 377-384.	1.9	11
178	Laser-induced nanoparticle ordering. Journal of Materials Research, 2002, 17, 2815-2822.	2.6	11
179	Micromechanical properties of a laser-induced iron oxide–aluminum matrix composite coating. Journal of Materials Research, 2003, 18, 833-839.	2.6	11
180	Effect of Surface Oxygen and Temperature on External and Micropore Adsorption of Water in Single-Walled Carbon Nanotubes by Gravimetric and Spectroscopic Experiments. Journal of Physical Chemistry C, 2009, 113, 12109-12117.	3.1	11

#	Article	IF	CITATIONS
181	Sublimation growth of titanium nitride crystals. Journal of Materials Science: Materials in Electronics, 2010, 21, 78.	2.2	11
182	Samarium electrodeposited acetate and oxide thin films on stainless steel substrate characterized by XPS. Surface Science Spectra, 2016, 23, 70-81.	1.3	11
183	Composition-Preserving Extraction and Characterization of Biomass Extrinsic and Intrinsic Inorganic Compounds. ACS Sustainable Chemistry and Engineering, 2020, 8, 1599-1610.	6.7	11
184	Atom- and cluster-assembled interfaces: Cr growth onBi2Sr2â^'xCa1+xCu2O8+y. Physical Review B, 1990, 41, 11677-11680.	3.2	10
185	The role of boron segregation in enhanced thermoelectric power factor of CoSi1â^'xBx alloys. Journal of Applied Physics, 2011, 110, 123711.	2.5	10
186	Novel Pulse Electrodeposited Co–Cu–ZnO Nanowire/tube Catalysts for C ₁ –C ₄ Alcohols and C ₂ –C ₆ (Except C ₅) Hydrocarbons from CO and H ₂ . Journal of Physical Chemistry C, 2012, 116, 10924-10933.	3.1	10
187	Surface-conductivity enhancement of PMMA by keV-energy metal-ion implantation. Nuclear Instruments & Methods in Physics Research B, 2014, 339, 75-84.	1.4	10
188	The impact of carbon coating on the synthesis and properties of α′′-Fe16N2 powders. Physical Chemistry Chemical Physics, 2016, 18, 13010-13017.	2.8	10
189	Kinetic and potential sputtering of an anorthiteâ€like glassy thin film. Journal of Geophysical Research E: Planets, 2017, 122, 1597-1609.	3.6	10
190	The response of ZrB2 to simulated plasma-facing material conditions of He irradiation at high temperature. Journal of Nuclear Materials, 2018, 507, 112-125.	2.7	10
191	Advancing Lithium- and Manganese-Rich Cathodes through a Combined Electrolyte Additive/Surface Treatment Strategy. Journal of the Electrochemical Society, 2019, 166, A3896-A3907.	2.9	10
192	Enhancing Cycling Stability and Capacity Retention of NMC811 Cathodes by Reengineering Interfaces via Electrochemical Fluorination. Advanced Materials Interfaces, 2022, 9, .	3.7	10
193	XPS study of chemical bonding at polyimide interfaces with metal and semiconductor overlayers. Vacuum, 1990, 40, 85-90.	3.5	9
194	CdTe(110) interface formation with reactive and nonreactive overlayers: Al, Ti, Pd, Ag, Au, In, and Ce. Journal of Vacuum Science and Technology A: Vacuum, Surfaces and Films, 1990, 8, 2055-2061.	2.1	9
195	Formation of Ultrasharp Vertically Aligned Cuâ^'Si Nanocones by a DC Plasma Process. Journal of Physical Chemistry B, 2006, 110, 4766-4771.	2.6	9
196	Large-grain poly-crystalline silicon thin films prepared by aluminum-induced crystallization of sputter-deposited hydrogenated amorphous silicon. Journal of Materials Research, 2006, 21, 761-766.	2.6	9
197	Understanding the Mechanism of Solventâ€Mediated Adhesion of Vacuum Deposited Au and Pt Thin Films onto PMMA Substrates. Advanced Functional Materials, 2013, 23, 1431-1439.	14.9	9
198	Tunable morphologies of indium tin oxide nanostructures using nanocellulose templates. RSC Advances, 2015, 5, 103680-103685.	3.6	9

#	Article	IF	CITATIONS
199	Surface chemistry and composition-induced variation of laser interference-based surface treatment of Al alloys. Applied Surface Science, 2019, 489, 893-904.	6.1	9
200	Investigation of Complex Intermediates in Solvent-Mediated Synthesis of Thiophosphate Solid-State Electrolytes. Journal of Physical Chemistry C, 2020, 124, 27396-27402.	3.1	9
201	Probing the Li ₄ Ti ₅ O ₁₂ Interface Upon Lithium Uptake by Operando Small Angle Neutron Scattering. ChemSusChem, 2020, 13, 3654-3661.	6.8	9
202	On the Production of X-rays by Low Energy Ion Beams. Scanning, 2007, 29, 1-4.	1.5	8
203	Tracer study of oxygen and hydrogen uptake by Mg alloys in air with water vapor. Scripta Materialia, 2015, 106, 38-41.	5.2	8
204	Wear penalty for steel rubbing against hard coatings in reactive lubricants due to tribochemical interactions. Tribology International, 2021, 160, 107010.	5.9	8
205	Surface reactivity and interface morphology for Ti growth on YBa2Cu3O7â^x, Y2BaCuO5, and CuO. Journal of Applied Physics, 1990, 67, 1995-2002.	2.5	7
206	An evaluation of phase separated, self-assembled LaMnO ₃ -MgO nanocomposite films directly on IBAD-MgO as buffer layers for flux pinning enhancements in YBa ₂ Cu ₃ O _{7-Î} coated conductors. Journal of Materials Research, 2010, 25, 437-443.	2.6	7
207	Hydrothermal Barium Titanate Thinâ€Film Characteristics and their Suitability as Decoupling Capacitors. Journal of the American Ceramic Society, 2010, 93, 2764-2770.	3.8	7
208	Surface-morphology changes and damage in hot tungsten by impact of 80 eV – 12 keV He-ions and keV-energy self-atoms. Journal of Physics: Conference Series, 2014, 488, 012036.	0.4	7
209	Controlling Water Vapor in Gas-Cell Microscopy Experiments. Microscopy and Microanalysis, 2018, 24, 286-287.	0.4	7
210	Growth and properties of Si–N–C–O nanocones and graphitic nanofibers synthesized using three-nanometer diameter iron/platinum nanoparticle-catalyst. Journal of Materials Research, 2005, 20, 850-855.	2.6	6
211	Analysis of copper treatments and the effects on signal propagation. , 2008, , .		6
212	Phase-Separated, Epitaxial, Nanostructured LaMnO ₃ +MgO Composite Cap Layer Films for Propagation of Pinning Defects in YBa ₂ Cu ₃ O _{7-1´} Coated Conductors. Applied Physics Express, 0, 2, 063008.	2.4	6
213	Microstructural Characterization of Ti-6Al-4V Metal Chips by Focused Ion Beam and Transmission Electron Microscopy. Metallurgical and Materials Transactions A: Physical Metallurgy and Materials Science, 2011, 42, 3527.	2.2	6
214	Highly Permeable Oligo(ethylene oxide)―co â€poly(dimethylsiloxane) Membranes for Carbon Dioxide Separation. Advanced Sustainable Systems, 2018, 2, 1700113.	5.3	6
215	Laser-interference pulse number dependence of surface chemistry and sub-surface microstructure of AA2024-T3 alloy. Optics and Laser Technology, 2020, 131, 106457.	4.6	6
216	RF sheath induced sputtering on Proto-MPEX part 2: Impurity transport modeling and experimental comparison. Physics of Plasmas, 2021, 28, 103508.	1.9	6

#	Article	IF	CITATIONS
217	Reaction and stability of metal/silicide interfaces: Ti/MoSi2 (001). Applied Physics Letters, 1990, 56, 671-673.	3.3	5
218	Comparison of the physical, chemical and electrical properties of ALD Al2 O3 on c- and m- plane GaN. Physica Status Solidi C: Current Topics in Solid State Physics, 2014, 11, 898-901.	0.8	5
219	Effect of Cold on the Microstructural Evolution and Integrity of a Sintered Silver Joint. Journal of Electronic Materials, 2017, 46, 4085-4092.	2.2	5
220	Materialâ€Dependent Antagonistic Effects between Soot and ZDDP. Advanced Materials Interfaces, 2020, 7, 1901956.	3.7	5
221	Temporal Evolution of Corrosion Film Nano-Porosity and Magnesium Alloy Hydrogen Penetration in NaCl Solution. Journal of the Electrochemical Society, 2020, 167, 131513.	2.9	5
222	Reduced Graphene Oxide Aerogels with Functionalization-Mediated Disordered Stacking for Sodium-Ion Batteries. Batteries, 2022, 8, 12.	4.5	5
223	Auger Microscopy of Laser Induced Fe Oxide/Al Reaction Composite Coating. Surface Engineering, 2004, 20, 48-52.	2.2	4
224	Wet-chemical synthesis of zirconium oxyfluoride. Journal of Materials Science, 2005, 40, 2655-2658.	3.7	4
225	The effect of hydrogen in the mechanism of aluminum-induced crystallization of sputtered amorphous silicon using scanning Auger microanalysis. Thin Solid Films, 2006, 510, 184-190.	1.8	4
226	Atomic layer deposition TiO2–Al2O3 stack: An improved gate dielectric on Ga-polar GaN metal oxide semiconductor capacitors. Journal of Vacuum Science and Technology B:Nanotechnology and Microelectronics, 2014, 32, 060602.	1.2	4
227	H/sub /spl alpha// emission as a feedback control sensor for reactive sputter deposition of nano-structured, diamond-like carbon coatings. IEEE Transactions on Plasma Science, 2005, 33, 799-807.	1.3	3
228	High-Resolution Mapping of the PFSA Polymer Distribution in PEFC Electrode Layers. ECS Transactions, 2014, 64, 819-827.	0.5	3
229	Samarium and europium beta―alumina derivatives characterized by XPS. Surface Science Spectra, 2016, 23, 102-111.	1.3	3
230	Chemical and Mechanical Analysis of HDIS Residues Using Auger Electron Spectroscopy and Nanoindentation. Solid State Phenomena, 0, 145-146, 261-264.	0.3	2
231	Low-temperature colossal carbon supersaturation enables anti-wear boundary film formation for austenitic stainless steels in oil-lubricated environment. Wear, 2011, 271, 1733-1738.	3.1	2
232	Structural Dependence of Grain Boundary Resistivity in Copper Nanowires. Japanese Journal of Applied Physics, 2011, 50, 08LB09.	1.5	2
233	X-Ray Photoelectron Spectroscopy (XPS). , 2013, , 4133-4138.		2
234	Corrosion Behavior of Zinc–Nickel and Graphene Layered Structures on Steel Substrates. Advanced Engineering Materials, 2019, 21, 1800949.	3.5	2

#	Article	IF	CITATIONS
235	Kinetics of borosilicate glass deposition. Journal of Materials Research, 2004, 19, 872-879.	2.6	1
236	Carbon Dioxide Separation: Highly Permeable Oligo(ethylene oxide)-co -poly(dimethylsiloxane) Membranes for Carbon Dioxide Separation (Adv. Sustainable Syst. 4/2018). Advanced Sustainable Systems, 2018, 2, 1870030.	5.3	1
237	Spectroscopic examinations of surface stability of high-temperature superconductors. AIP Conference Proceedings, 1988, , .	0.4	0
238	Interface formation: High-temperature superconductors with noble metals, reactive transition metals, and semiconductors. AIP Conference Proceedings, 1988, , .	0.4	0
239	XPS Analysis of Fuel Cell Membrane Prepared Using an Ultra-Low-Angle-Microtomy Technique. Microscopy and Microanalysis, 2009, 15, 1130-1131.	0.4	0
240	Kinetic and potential sputtering of lunar regolith: The contribution of the heavy (minority) solar wind ions. , 2013, , .		0
241	Model "Alloy―Specimens for MEMS-Based Closed-Cell Gas-Reactions. Microscopy and Microanalysis, 2017, 23, 908-909.	0.4	0
242	Fluorination of MXene by Elemental F ₂ as Electrode Material for Lithiumâ€lon Batteries. ChemSusChem, 0, , .	6.8	0
243	Fluorination of MXene by Elemental F 2 as Electrode Material for Lithiumâ€lon Batteries. ChemSusChem, 2019, 12, 1271-1271.	6.8	0